LASER & PHOTONICS REVIEWS
www.lpr-journal.org

Rewritable ITO Patterning for Nanophotonics

*Xinqin Liu, Pan Peng, Zhenyang Zhang, Xiangyu Zhao, Wenyu Chen, Shiyuan Liu, and Jinlong Zhu**

Nanophotonic devices leverage unique interactions between photons and materials at the nanoscale, enabling applications in optical communication, biosensing, and quantum computing. These devices' properties are susceptible to material composition and structural design. Nanofabrication techniques, such as optical lithography, e-beam lithography, two-photon polymerization, and direct laser writing, have been widely applied to fabricate nanophotonic devices. Notably, rewritable fabrication stands out due to its low cost, flexibility, efficiency, and multi-functionality. In this paper, a novel rewritable nanofabrication technique is proposed, which combines electrochemical reactions with direct laser writing, to fabricate nanophotonic devices on low-cost indium tin oxide (ITO) films. The experimental results have demonstrated that high-quality and erasable photonic structures such as diffraction gratings and holography masks can be directly fabricated using our technique. Hence, it is believed that this method can be applied in diverse fields such as nanophotonics, optoelectronic devices, biosensors, micro-electromechanical systems, and nonlinear optics.

1. Introduction

Nanophotonic devices, which could precisely manipulate electromagnetic waves at a sub-wavelength scale, have been applied in diverse disciplines:[1] Metamaterials, which rely on the layout of specifically designed patterns, have unique electromagnetic response characteristics that can change and control exotic optical phenomena.[2] Photonics-based chemical and biological sensors, which take advantage of surface-enhanced Raman scattering on a roughened or nanostructured substrate, could detect and analyze low concentrations of substances.[3] Photonic integrated circuits (PIC), which integrate multiple optical functions on a single chip, could enable on-chip phase measurement,[4,5] nanosensing,[6,7] and large-scale artificial intelligence.[8,9] To fabricate nanophotonic devices, conventional nanofabrication techniques, such as optical lithography,[10,11] electron-beam lithography,[12] two-photon polymerization (TPP) printing,[13,14] direct laser writing (DLW),[15,16] direct ink writing,[17,18] laser-induced forward transfer,[19,20] laser-assisted electrophoretic deposition,[21–23] and laser-induced microbubble technique,[24,25] have been widely applied. Among all the nanofabrication methods, the erasable and rewritable ones are of great interest to researchers because of the merits of low cost, flexibility, efficiency, and multiple functions.[26–32] For example, DLW combined with phase change materials heat annealing can achieve flexible PIC patterning,[33–36] and rewritable color nanoprints in a cheap and fast manner.[37] Light-induced nanowetting uses projection lithography and template-wetting methods to achieve erasable and rewritable polymer nanoarrays via solid-to-liquid transitions.[38] Moreover, it has been realized that plasma etching combined with UV-curable resin can manufacture core–shell magnetic micropillars for programmable actuation.[39] Therefore, a low-cost and rewritable fabrication technique for nanophotonic devices is very important.

Indium tin oxide (ITO), which mainly consists of In_2O_3 and SnO_2 at the mass percentage of 9:1,[40] has many favorable properties such as high conductivity ($\approx 5 \times 10^{-4}$ Ω cm),[41] high transparency (≈98% optical transmittance),[42] good wear resistance and adhesion on glass,[43] and wide band gap (3.5–3.7 eV).[44] As a result, it has been used in many fields such as solar cells,[45] electrochromic glasses,[46] liquid crystal display devices,[47] surface-enhanced Raman spectroscopy,[48] electrophoretic deposition,[49] and micro-nano fabrication.[21–23] ITO is usually prepared by reactive magnetron sputtering as a continuous thin film coated on glass or polyethylene terephthalate.[50] To satisfy specific applications, nanofabrication techniques have been applied to make functional structures on ITO thin films, such as the manufacture of touch screens and OLEDs,[51,52] passive elements and sensors in cryogenic systems,[53,54] transparent microelectrode structures,[55] and transparent gas flow meter.[56] It has been demonstrated that 92.7% enhancement in solar cell photoelectric conversion efficiency after ITO surface treatments,[57] and

X. Liu, P. Peng, Z. Zhang, X. Zhao, W. Chen, J. Zhu
State Key Laboratory of Intelligent Manufacturing Equipment and Technology
Huazhong University of Science and Technology
Wuhan 430074, China
E-mail: jinlongzhu03@hust.edu.cn
S. Liu, J. Zhu
State Key Laboratory of Intelligent Manufacturing Equipment and Technology
Huazhong University of Science and Technology
Research Institute of Huazhong University of Science and Technology
Shenzhen
Optics Valley Laboratory
Wuhan 430074, China

The ORCID identification number(s) for the author(s) of this article can be found under https://doi.org/10.1002/lpor.202401799

DOI: 10.1002/lpor.202401799

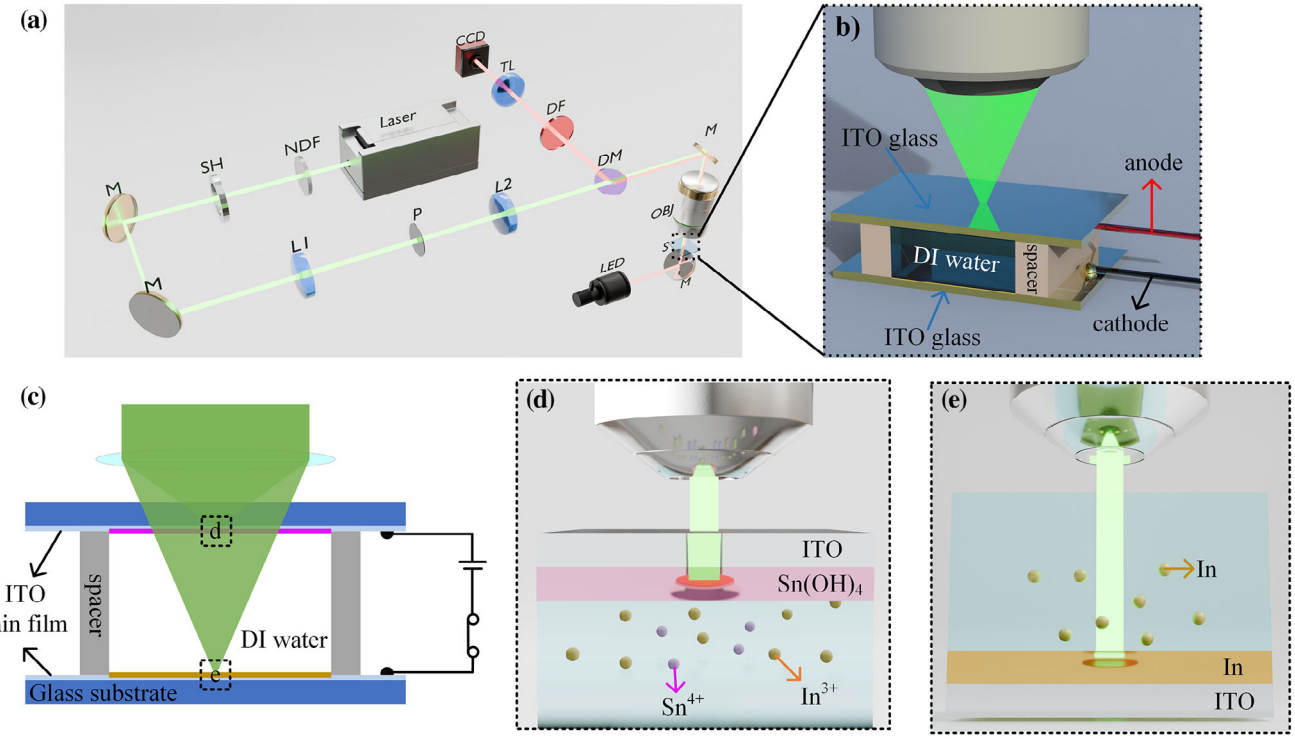

Figure 1. Principle and schematic diagram of the proposed rewritable ITO nanopatterning method. a) Schematic of the experimental setup. NDF, neutral density filter; SH, shutter; M, mirror; L, lens; P, pinhole; DM, dichroic mirror; OBJ, objective lens; S, sample; DF, dichroic filter; TL, tube lens. b) A zoomed-in figure shows the experimental chamber consisting of ITO glass, spacer, DI water, and wires connected to the ITO glass. c) Schematic diagram of the ITO patterning process. The laser was focused on either the top or bottom side of the ITO film for direct patterning. d,e) $Sn(OH)_4$ and In layers are formed on the ITO bulk after applying voltage. The laser-induced hydrothermal reaction of $Sn(OH)_4$ and thermal ablation of In result in the patterned structure on ITO thin film.

multiple sample detection could be achieved simultaneously on one substrate using a nano-dot array on ITO films.[48]

In this paper, we propose a rewritable ITO patterning technique, which uses the principles of electrochemical reactions and DLW, for erasable nanophotonic applications. Using a low-power continuous wave (CW) laser, our technique could achieve ITO nanopatterning under both anodic and cathodic polarization. We successfully validated the write, erase, and rewrite of photonic structures, which demonstrated our method as a low-cost (99.5% reduction in energy consumption compared to ultrafast pulse laser),[58] easy-to-operate (only requires heat annealing for pattern erase) and environment friendly (water required only) technique for nanophotonics.

2. Results and Discussion

The schematic of our experimental system is presented in **Figure** 1a. A 532 nm CW laser (MLL-FN-532, Changchun New Industries Optoelectronics Tech. Co., Ltd, China) was used as the DLW source. The power was attenuated to 3–5 mW after passing through the objective (Nikon, TU Plan ELWD, ×50, NA 0.6) using a neutral density filter. An optical shutter and two 45° reflective mirrors were used to switch the laser on or off and to control the laser direction, respectively. The laser was focused on the surface of the ITO thin film by the objective after passing lens 1, the pinhole, lens 2, the dichroic mirror, and the reflective mirror. An in situ microscope system consisting of the 660 nm LED (LEM-660C1, JCOPTIX, China), the objective, and the tube lens were used to observe the patterning process. A dichroic filter was used to prevent the focused green laser from entering the CCD camera. Commercially available ITO glass (MJY, Foshan Yuanjingmei Glass Co., Ltd, China) with sizes 40 × 40 × 1.1 mm and 15 × 15 × 1.1 mm, were utilized in our experiments. The thickness, resistance, and transmissivity are 185 ± 20 nm, 10 Ω, and 84%, respectively. The ITO sample is conductive only on one side. It was cleaned sequentially with methylbenzene, acetone, and ethyl alcohol, followed by a rinse with deionized (DI) water. A 100 um-thick cavity was sandwiched between two ITO-coated glass substrates using double-sided tape, and DI water was injected into the cavity via capillary force. Subsequently, a metal wire was connected to the ITO film by copper conductive tape, after which a microelectrochemical cell was completed as presented in Figure 1b. The sample mounted on the XYZ stage (EMLSS90-100C1, LBTEK, China) was connected to a DC voltage supply through crocodile clips. The voltage was set from 2.8 to 3.5 V, such that the electrochemical reaction between ITO and DI water could be realized. See Figure 1c. $Sn(OH)_4$ and In layers are formed on the ITO thin film at anodic and cathodic polarization, respectively. Because $Sn(OH)_4$ and In have a much higher light absorption rate and a lower melting point than those of the ITO film, they can be easily patterned by a low-power CW laser. See the schematic in Figure 1d,e. Scanning electron microscopy (SEM)

and energy-dispersive spectrometer (EDS) measurements were performed on Zeiss GeminiSEM300 to analyze the patterned ITO structures.

TPP is a nonlinear fabrication method,[59] that takes advantage of two photons' energy absorbed simultaneously to stimulate the polymerization reaction of the photosensitive materials. It can fabricate 3D components inside the material with high precision and resolution over the optical diffraction limit. Meanwhile, a high-power ultra-fast pulse femtosecond laser is necessary to realize the nonlinear two-photon absorption, and printable materials are mainly transparent photosensitive polymer resins.[60] DLW is a universal micro-nano fabrication technique. Due to the high transparency of the ITO, it is difficult to directly ablate ITO with a CW laser because of the weak linear absorbance and high material ablation threshold.[61] Consequently, whether direct laser thermal ablation[62–64] or laser-induced ITO crystallization followed by anisotropic chemical wet etch,[65–67] pulse ultrafast laser is necessary, such as nanosecond,[56] femtosecond[68] and picosecond lasers.[58] To our knowledge, CO_2 CW laser with power ranging from 1 to 10 watts was primarily used for ITO thin film annealing to improve surface quality and optical-electrical properties rather than pattern generation.[44]

To pattern ITO thin film by a low-power CW laser, we take advantage of an electrochemical reaction rather than the pulse-laser-based physical ablation and thermal melting. Generally speaking, the mechanisms of electrochemical corrosion at the anodic and cathodic polarization are different.[69–79] Kraft et al. found it has oxygen evolution accompanied by electrode corrosion after strong anodic polarization (greater than 1.5 V vs a saturated calomel electrode) in aqueous electrolytes.[70] He revealed the underlying process involved in the corrosion of ITO anodic oxygen evolution. This process starts from the breaking of In-O and Sn-O bonds at the surface of the ITO, after which In^{3+} ions are released into the solution. Meanwhile, the more amphoteric Sn^{4+} ions react with OH^- ions, forming a thin layer of $Sn(OH)_4$ or SnO_2 on the ITO surface, but there is no change in the bulk ITO. As for the cathodic polarization,[48,72,75,78] an obvious electrochemical corrosion phenomenon along with a layer of yellow-colored substance coated on the surface of ITO film can be observed, which is proved to be a metallic mirror composed primarily of In and a small amount of Sn.[73,74,78] This coating leads to a decrease in the transmissivity of the ITO film. Although the formation of the metallic mirror may cause the electrical and optical properties of ITO thin film to deviate, there are still some interesting applications. For instance, it can enable large-area and patternable nano-dot arrays for surface-enhanced Raman spectroscopy.[48] Meanwhile, electrochemically reduced ITO exhibits excellent non-linear optical performance, with the transmittance tunable by reduction potential and processing time.[76,79] Specifically, considering ITO has a vanishingly small real part of the dielectric constant within the near-infrared wavelength range, known as epsilon-near-zero properties, which endow ITO with high nonlinear conversion efficiency at the nanoscale.[80] Consequently, metal-coated ITO can serve as perfect absorption thin film in optical filters and optical switches/modulators, [81,82] while patterned ITO thin film can be used to generate nonlinear photoluminescence[83] and terahertz wave with complete phase and amplitude control.[84–86]

The focused spot of a 5 mW CW laser cannot trigger the ablation of the ITO surface. See the experimental results in Figure S1 (Supporting Information). However, the laser spot starts to generate patterns as it scans over the ITO surface by applying a DC voltage on the ITO surface. It should be emphasized that the moderate increase of the laser power over 5 mW will not cause thermal damage on the ITO surface, but it may boil the water and generate bubbles. Similarly, increasing the DC voltage over 3.5 V also generates many bubbles owing to the electrolysis of water. Hydrogen and oxygen are formed at positive and negative electrodes, respectively. This can impede the patterning process. The working principle of the electrically controlled ITO patterning can be explained as follows: Although low-power CW laser cannot directly ablate the ITO thin film because In_2O_3 and SnO_2 in the ITO thin film corresponding to the melting points of 2000 and 1630 °C, respectively, the electrochemical reaction can significantly reduce the energy required in this process, which is similar to the photoelectrochemical etching process.[87] There will be oxygen corrosion of the ITO electrode once the anodic polarization is applied to the ITO thin film. Because the further oxidation of In^{3+} and Sn^{4+} is impossible, the only component in the ITO that can be oxidized is oxygen (O^{2-}), which will become O_2. The electrochemical reaction under anodic polarization can be described using Equations (1) and (2), i.e.,

$$2In_2O_3 \rightarrow 4In^{3+} + 3O_2(g) + 12e^- \quad (1)$$

$$SnO_2 + 4OH^- \rightarrow Sn(OH)_4 + O_2(g) + 4e^- \quad (2)$$

Further experiments were conducted by recording the γ spectra of the ITO thin film before anodization and the electrolyte after anodization, as discussed in Reference.[70] It was observed that the mass content of In in the electrolyte was significantly higher than that of Sn. This suggested that more In^{3+} ions migrated into the solution during anodization, while Sn^{4+} ions accumulated on the ITO surface. Sn^{4+} reacts with OH^- to form the hydrated species $Sn(OH)_4$, which finally generates SnO_2 after the voltage is off due to its higher stability than that of $Sn(OH)_4$. Moreover, it has been confirmed that the mass ratio of In/Sn in the ITO thin film before anodization was higher than that after anodization (as shown in **Figure 2a** and the EDS measurement results in Figure S2, Supporting Information of the Supplemental Material). Therefore, we can confirm that a $Sn(OH)_4$ layer was indeed deposited on the surface of the bulk ITO, which hinders further anodic oxygen corrosion, provided when continuous DC voltage was applied. Because the melting point of $Sn(OH)_4$ is much lower than those of SnO_2 and In_2O_3, it can be directly ablated by a low-power CW laser. As a result, we can achieve the ITO patterning at the positive electrode. When a cathodic polarization was applied to the ITO thin film, the chemical reaction can be described by the following equation:

$$In_2O_3 + 3H_2O + 6e^- \rightarrow 2In + 6OH^- \quad (3)$$

In_2O_3 was reduced into metal In, which was deposited on the surface of ITO thin film. This can be confirmed by Figure 2a, in which the oxygen content was less than that of the case without reaction. Moreover, it can be observed that the ITO glass became bronze, while there is no apparent color change under

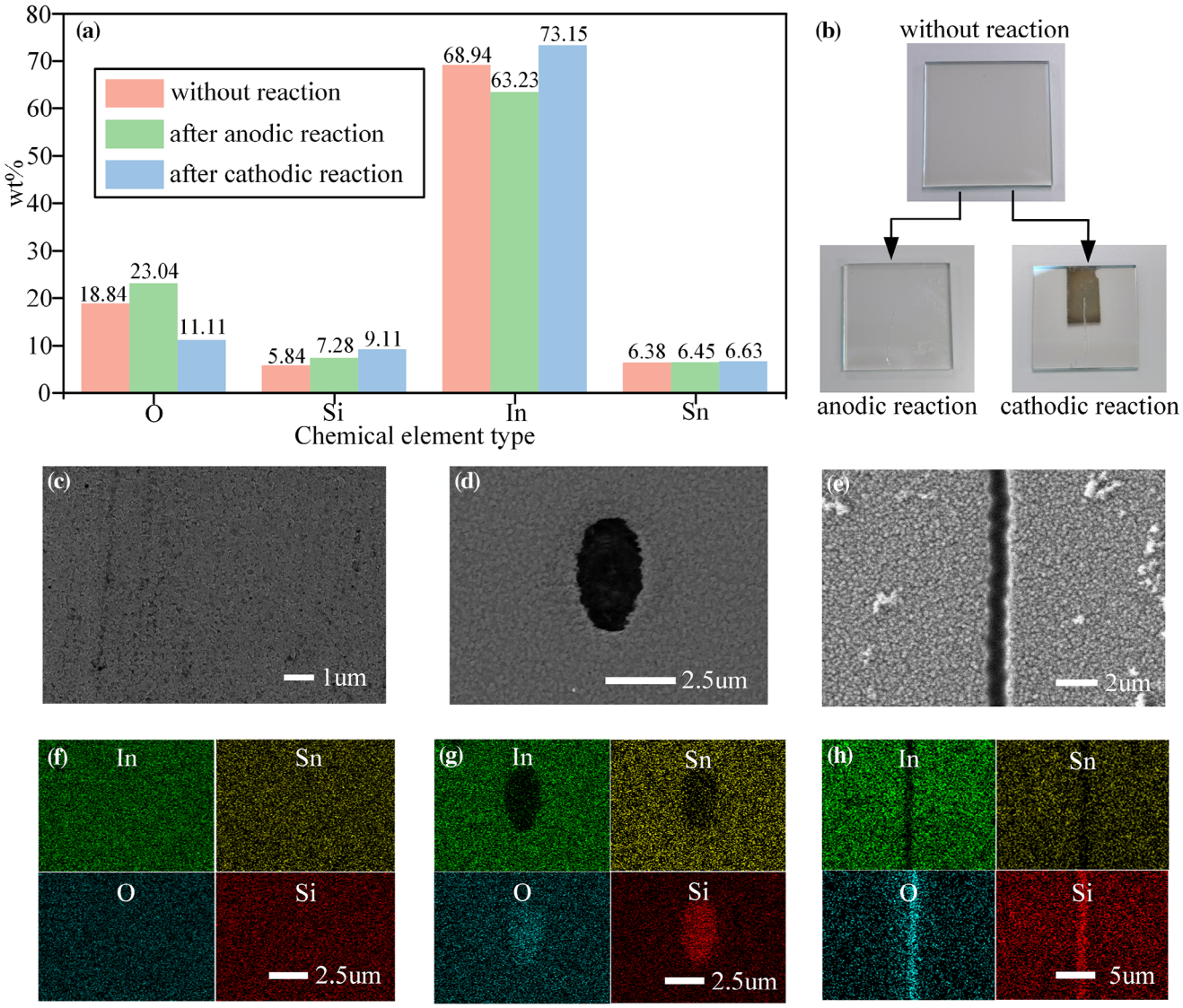

Figure 2. Experimental results analysis for ITO thin films before and after the nanopatterning process. a) EDS analysis results of the ITO thin films before and after electrochemical reactions. b) The optical images of ITO glass after electrochemical reactions. c,d,e) SEM images of the ITO thin films without any reaction, after patterning during the anodic reaction and cathodic reaction, respectively. f,g,h) EDS maps of the four chemical elements In, Sn, O, and Si in ITO glass.

anodic polarization.[76,48] See the results in Figure 2b. Because the melting point of In is 156 °C, it can be easily ablated by a low-power CW laser writing. SEM measurements for ITO thin films without reaction and after surface patterning at anodic and cathodic polarization are presented in Figure 2c,d, and e. The corresponding EDS maps for In, Sn, O, and Si elements are shown in Figure 2f,g,h. It can be observed from Figure 2d that there was not any apparent change in ITO surface morphology outside the central hole when compared to the unprocessed ITO surface in Figure 2c. However, we observed many nano-dots (NDs) on the ITO surface at cathodic polarization in Figure 2e, which had also been confirmed by many other studies.[72–75,78,79] As for the EDS maps of the ITO glass without reaction shown in Figure 2f, it can be seen that In, Sn, O, and Si elements are all uniformly distributed. However, In and Sn elements in the central hole area are much less than those in the background area, while O and Si elements are not. A similar phenomenon can also be observed in Figure 2h. This indicates that the patterned ITO was indeed removed by low-power CW laser writing and the glass substrate was exposed. Meanwhile, 3D images and the corresponding cross-sections of the patterned ITO were measured through quadri-wave lateral shearing interferometry shown in Figure S3 (Supporting Information). It can be seen that the uniformity of the ITO surface after the anodic reaction was better and smoother than that after the cathodic reaction, causing the coating of In NDs. CW laser direct writing achieved 2.5 um full width at half maximum (FWHM) under a 50× objective lens. It is suggested that the objective lens with a higher NA, a laser with a shorter wavelength, and a femtosecond laser be considered to reduce the heat effect and improve the resolution. Gaussian outlines

corresponding to the shape of the laser focus were generated in the written area. At the same time, no apparent changes occurred in the unwritten area, and the maximum writing area only depends on the travel range of the XY displacement stage.

More complex patterns such as dots array and logo "HUST" can be directly patterned on ITO thin film under anodic and cathodic polarization. See Figure S4 (Supporting Information). We should emphasize that small cracks may exist in the patterned area at anodic polarization when laser power is high (but before generating bubbles); see the high-magnification SEM image of a single dot in Figure S4 (Supporting Information). These cracks were usually observed on the ITO thin film surface after laser annealing, as discussed in References [44,55]. These micro-cracks resulted from different residual tension stress of the crystalline phase transformation between irradiated and non-irradiated regions of the ITO thin film.[88] However, in this study, cracks were caused by different residual tension stress of $Sn(OH)_4$ and SnO_2 during the chemical dynamic transition under anodic polarization. It was suggested that a higher laser repetition rate and moderate laser power can reduce the formation of micro-cracks.[65] Other potential factors that may influence the fabrication results include the thickness and composition of ITO and solution composition. If ITO film is too thin, inadequate $Sn(OH)_4$ and In are generated for nanopatterning, reducing the erasable patterning times and rewritable performance. Considering the stability of SnO_2 against anodic dissolution during oxygen evolution, highly doped SnO_2 layers are probably suitable for electrochemical corrosion protection purposes.[70] In contrast, lowly doped SnO_2 makes it challenging to pattern on ITO at anodic polarization because patternable product $Sn(OH)_4$ is reduced. Therefore, there would be a tradeoff in the content of SnO_2. On the other hand, due to the high proportion of In_2O_3 in ITO and the fact that it primarily works during the cathodic reaction, there are a lot of allowances for the content of In_2O_3 as long as it can produce adequa te reduced metal indium for nanopatterning. Lastly, the electrolyte solution also plays an important role; for example, if NaCl solution is used for an electrochemical reaction, $SnCl_4$ is produced, preventing $Sn(OH)_4$. Therefore, the ITO electrode is totally destroyed, finally causing both In^{3+} and Sn^{4+} to pass into the solution.[70]

To validate the potential of the proposed ITO patterning technique in nanophotonics, we fabricated diffraction gratings with three different periods (i.e., 20, 10, and 5 um) on ITO thin film under cathodic polarization. See the left column in **Figure 3**a–c. The optical images of the entire grating areas and the details of gratings were obtained using a low-NA objective (Zeiss, N-Achroplan, ×2.5, NA 0.07) and a high-NA objective (Olympus, LMPlanFLN, ×20, NA 0.40), respectively. The gratings diffraction patterns from the 532 nm laser were captured by a CMOS camera (Prosilica GT 1930, Allied Vision, TKH Technology Company). We captured independent frames at three different positions followed by image stitching to obtain the entire diffraction pattern. It can be seen from the middle column in Figure 3a–c that the intensity of the high diffraction orders was significantly weaker than that of the zeroth order, leading to a low image contrast. The log operation was applied to the diffraction patterns to enhance visibility. The right column in Figure 3a–c presents the cross-sections of the normalized experimental and simulated diffraction patterns. The grating equation at a normal incidence is given by

$$P \sin \theta_m = m\lambda \tag{4}$$

where P is the grating period, λ is the incident wavelength, m is the diffraction order, and θ_m is the diffraction angle corresponding to the m^{th} order. It can be derived from Equation (4) that a smaller P results in a larger θ_{m} for a given λ and m. This was experimentally confirmed in Figure 3a,b,c that reducing P from 20 to 5 µm increased the first-order diffraction angle θ_1. Meanwhile, a quantitative comparison was conducted between fabricated gratings and grating equations to demonstrate the precision of ITO patterning. Both the cross-sections of the normalized diffraction patterns in Figure 3 and the experimentally obtained diffraction angles in Figure S5 (Supporting Information) match well with the theoretical predictions, indicating that the proposed method could generate high-quality nanopatterns. Moreover, we fabricated a transmissive holography mask on ITO thin film as an example for complex nanopatterns. The holography mask is the most critical element used in holography lithography, which is a technique different from conventional projection lithography. Image information is recorded into the holography mask. Images can be generated by illuminating the holography mask through a coherent laser, as illustrated in Figure 3d. The computer-generated hologram is presented in Figure 3g. Figure 3e is the fabricated holography mask according to the computer-generated hologram, using our proposed ITO patterning technique. Figure 3f presents the zoomed-in view of the feature details on the mask. Figure 3h presents the holography image captured by the camera, which consists of five parallel lines. Subsequently, we also fabricated another holography mask with 200 × 200 pixels; see Figure S6 (Supporting Information). It can be concluded that a high-resolution holography mask could improve the quality of the holographic reconstruction image.

The patterned nanostructures on ITO thin film can be erased through annealing, i.e., annealing the patterned ITO thin film on a hot plate at 200 °C to melt and oxidize In into In_2O_3, after which we can re-write patterns on the same area of the ITO thin film, see the flow diagram in Figure S7 (Supporting Information). To validate this, we wrote, erased, and re-wrote a symbol "+" on ITO thin film. See the optical images in **Figure 4**a–d. Meanwhile, we fabricated an orthogonal grating area (see Figure 4e–h) and compared the corresponding diffraction patterns before and after the re-writing to further validate the reversibility. See the diffraction patterns in Figure 4i,j and the cross-sections in Figure 4k. The diffraction patterns corresponding to the first write and re-write match very well, especially at the lower diffraction orders. The minor difference with 7.08% root mean square error (RMSE) at the higher diffraction orders could be attributed to the experimental errors and changes in surface thickness, roughness, and transmittance caused by the melted In and the newly deposited In. To further explore the maximum number of rewriting cycles and the effects of each cycle, we measured the transmittance of the pristine ITO at each cycle as shown in Figure 4l. It can be seen that the pristine ITO transmittance was 85% at 532 nm wavelength. The transmittance reduced to 40% through the first cathodic reaction for laser direct writing and it recovered to 77% after an

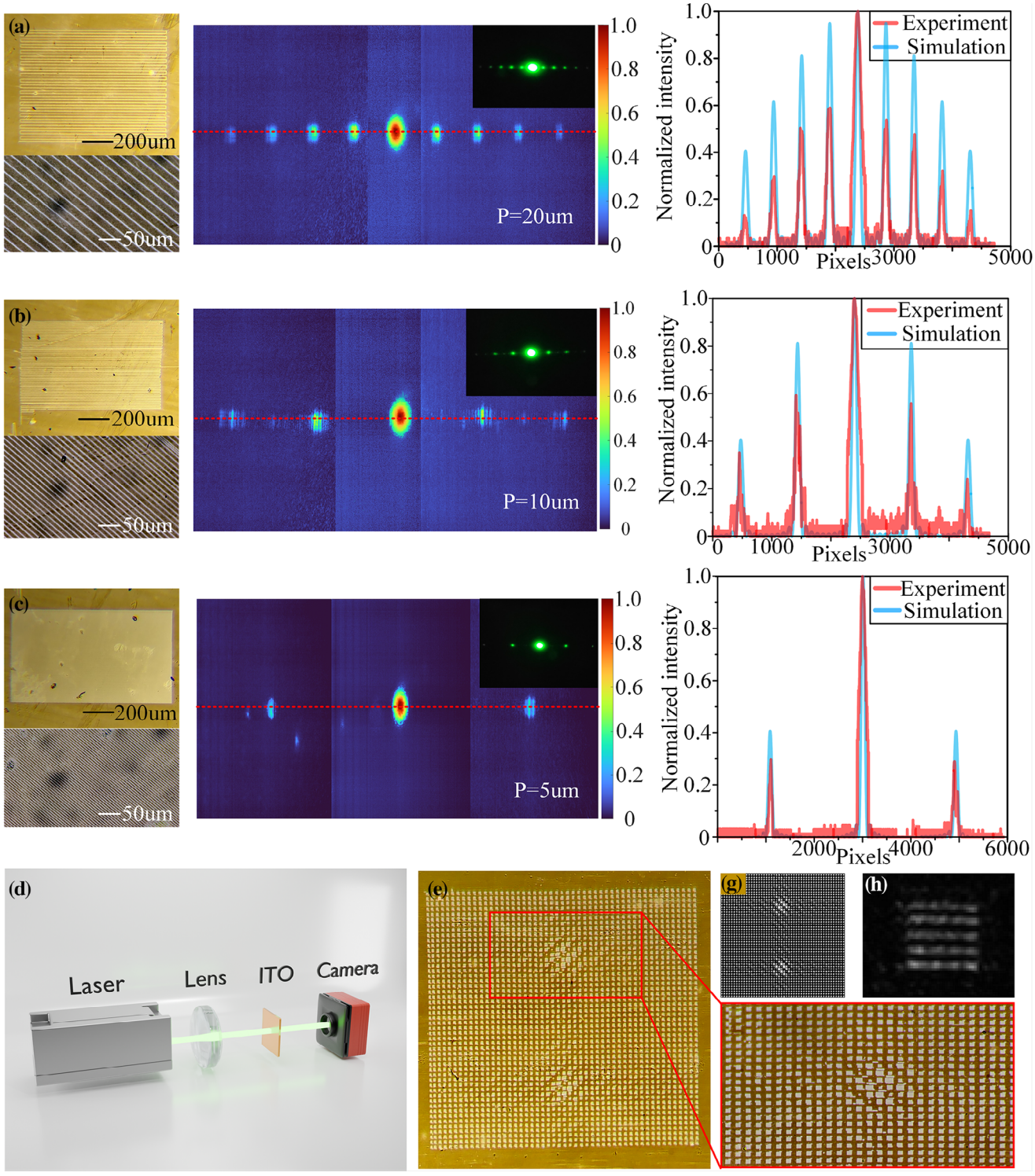

Figure 3. Nanophotonic devices patterned on the ITO thin film and the corresponding diffraction results. a–c) The fabricated diffraction gratings with three different periods, i.e., 20, 10, and 5 um. The middle column presents the diffraction patterns captured by the camera. The right column presents the cross-sections of the normalized experimental and simulated diffraction patterns. d) The optical configuration to validate the performance of the fabricated holography mask. e) The fabricated holography mask and f) the zoomed-in view showing the feature details. g) The computer-generated hologram with 500 × 500 pixels. h) The holographic reconstruction image (i.e., raster lines) captured by the camera in (d).

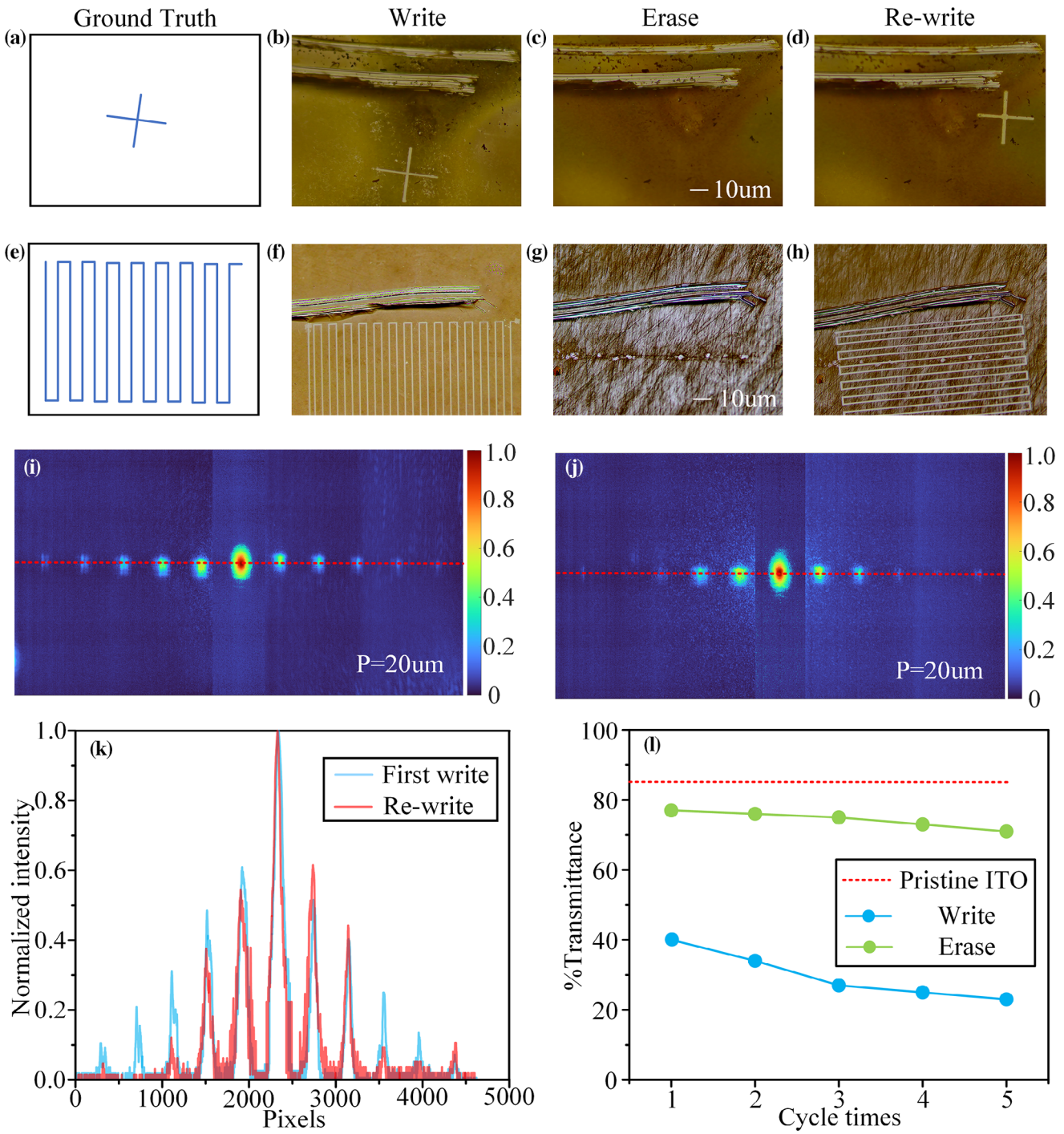

Figure 4. Reversible nanostructure patterning on ITO thin films. a) Ground truth of the symbol "+". Optical images of the "+" symbol in the processes of b) write, c) erase, and d) re-write. e) Ground truth of a grating. Optical images of the grating in the processes of f) write, g) erase, and h) re-write. i–k) The diffraction patterns and the corresponding cross-sections after writing and re-writing. l) The transmittance as a function of rewriting cycles.

anneal process for erasing. The theoretical maximum number of rewriting cycles depends on the transmittance difference between write and erase, so the ITO patterning is rewritable as long as they don't coincide. However, as the cycle times increased, the transmittance after writing and erasing decreased, which might result from increased surface roughness and inadequate melting and oxidation process of the indium thin layer during annealing. Meanwhile, this might reduce the uniformity of the reduced ITO surface indium thin layer, influencing the cycle times and rewriting performance. This situation may be alleviated by adjusting some experimental parameters such as electrochemical reaction time, voltage, anneal time and temperature. We want to

leave this as an open question shortly and make further studies on this topic.

3. Conclusion

In this paper, we propose a rewritable, cost-efficient, and easy-to-operate ITO nanopatterning technique, which combines electrochemical reactions with direct laser writing, for nanophotonic applications. We experimentally fabricated diffraction gratings with various pitches and holography masks with different resolutions using the proposed technique. Our experimental tests for the fabricated photonic structures demonstrated that their performance matched well with the theoretical predictions under multiple cycles. We believe that our method holds potential for applications in various fields, such as metasurfaces, optoelectronic devices, biosensors, nonlinear optics, optical imaging, and clean energies.

Supporting Information

Supporting Information is available from the Wiley Online Library or from the author.

Acknowledgements

X.L. and P.P. contributed equally to this work. This work was funded by the National Nature Science Foundation of China (Grant No. 52450158 and 52175509), the National Key Research and Development Program of China (2023YFF1500900), the Shenzhen Fundamental Research Program (JCYJ20220818100412027), the Guangdong-Hong Kong Technology Cooperation Funding Scheme Category C Platform (SGDX20230116093543005), and the Innovation Project of Optics Valley Laboratory (Grant No. OVL2023PY003). Thanks engineers Pan Li in Optoelectronic Micro & Nano Fabrication and Characterizing Facility, Wuhan National Laboratory for Optoelectronics of Huazhong University of Science and Technology for the support in device fabrication.

Conflict of Interest

The authors declare no conflict of interest.

Data Availability Statement

The data that support the findings of this study are available from the corresponding author upon reasonable request.

Keywords

electrochemical reaction, laser writing, nanophotonics, rewritable fabrication

Received: October 26, 2024
Revised: January 11, 2025
Published online: February 4, 2025

[1] J. E. Melzer, E. McLeod, *Nanophotonics.* **2020**, *9*, 1373.
[2] C. M. Soukoulis, M. Wegener, *Nat. Photon.* **2011**, *5*, 523.
[3] J. Langer, D. Jimenez De Aberasturi, J. Aizpurua, R. A. Alvarez-Puebla, B. Auguié, J. J. Baumberg, G. C. Bazan, S. E. J. Bell, A. Boisen, A. G. Brolo, J. Choo, D. Cialla-May, V. Deckert, L. Fabris, K. Faulds, F. J. García De Abajo, R. Goodacre, D. Graham, A. J. Haes, C. L. Haynes, C. Huck, T. Itoh, M. Käll, J. Kneipp, N. A. Kotov, H. Kuang, E. C. Le Ru, H. K. Lee, J.-F. Li, X. Y. Ling, et al., *ACS Nano.* **2020**, *14*, 28.
[4] M. Song, J. Steinmetz, Y. Zhang, J. Nauriyal, K. Lyons, A. N. Jordan, J. Cardenas, *Nat. Commun.* **2021**, *12*, 6247.
[5] Y. Yang, M. Turchetti, P. Vasireddy, W. P. Putnam, O. Karnbach, A. Nardi, F. X. Kärtner, K. K. Berggren, P. D. Keathley, *Nat. Commun.* **2020**, *11*, 3407.
[6] A. Lay-Ekuakille, A. Massaro, S. P. Singh, I. Jablonski, M. d. Z. U. Rahman, F. Spano, *IEEE Sensors J.* **2021**, *21*, 12645.
[7] P. Steglich, G. Lecci, A. Mai, *Sensors.* **2022**, *22*, 2901.
[8] S. Ning, H. Zhu, C. Feng, J. Gu, Z. Jiang, Z. Ying, J. Midkiff, S. Jain, M. H. Hlaing, D. Z. Pan, R. T. Chen, *J. Lightwave Technol.* **2024**, *42*, 7834.
[9] B. J. Shastri, A. N. Tait, T. Ferreira De Lima, W. H. P. Pernice, H. Bhaskaran, C. D. Wright, P. R. Prucnal, *Nat. Photonics.* **2021**, *15*, 102.
[10] L. F. Thompson, C. G. Willson, M. J. Bowden, *Introduction to Microlithography: Theory, Materials, and Processing*, American Chemical Society, WASHINGTON, D C **1983**.
[11] T. Ito, S. Okazaki, *Nature.* **2000**, *406*, 1027.
[12] A. A. Tseng, K. Chen, C. D. Chen, K. J. Ma, *IEEE Trans. Electron. Packag. Manufact.* **2003**, *26*, 141.
[13] X. Zhou, Y. Hou, J. Lin, *AIP Adv.* **2015**, *5*, 030701.
[14] B. H. Cumpston, S. P. Ananthavel, S. Barlow, D. L. Dyer, J. E. Ehrlich, L. L. Erskine, A. A. Heikal, S. M. Kuebler, I.-Y. S. Lee, D. McCord-Maughon, J. Qin, H. Röckel, M. Rumi, X.-L. Wu, S. R. Marder, J. W. Perry, *Nature.* **1999**, *398*, 51.
[15] Y.-L. Zhang, Q.-D. Chen, H. Xia, H.-B. Sun, *Nano Today.* **2010**, *5*, 435.
[16] Z. Ma, Y. Zhang, B. Han, Q. Chen, H. Sun, *Small Methods.* **2018**, *2*, 1700413.
[17] J. A. Lewis, *Adv. Funct. Mater.* **2006**, *16*, 2193.
[18] J. A. Lewis, J. E. Smay, J. Stuecker, J. Cesarano, *J. Am. Ceram. Soc.* **2006**, *89*, 3599.
[19] M. Feinaeugle, R. Pohl, T. Bor, T. Vaneker, G. Römer, *Addit. Manuf.* **2018**, *24*, 391.
[20] C. W. Visser, R. Pohl, C. Sun, G. Römer, B. Huis In 'T' Veld, D. Lohse, *Adv. Mater.* **2015**, *27*, 4087.
[21] Y. Yoshimoto, K. Nakazawa, M. Ishikawa, A. Ono, F. Iwata, *Opt. Express.* **2023**, *31*, 41726.
[22] T. Takai, H. Nakao, F. Iwata, *Opt. Express.* **2014**, *22*, 28109.
[23] K. Nakazawa, S. Ozawa, F. Iwata, *Nanomanuf. Metrol.* **2021**, *4*, 271.
[24] L. Lin, X. Peng, Z. Mao, W. Li, M. N. Yogeesh, B. B. Rajeeva, E. P. Perillo, A. K. Dunn, D. Akinwande, Y. Zheng, *Nano Lett.* **2016**, *16*, 701.
[25] B. Bangalore Rajeeva, L. Lin, E. P. Perillo, X. Peng, W. W. Yu, A. K. Dunn, Y. Zheng, *ACS Appl. Mater. Interfaces.* **2017**, *9*, 16725.
[26] T. Lv, Z. Cheng, D. Zhang, E. Zhang, Q. Zhao, Y. Liu, L. Jiang, *ACS Nano.* **2016**, *10*, 9379.
[27] Z. Wang, S. Zhang, B. Tang, *ACS Nano.* **2024**, *18*, 186.
[28] S. Cui, L. Qin, X. Liu, Y. Yu, *Adv. Opt. Mater.* **2022**, *10*, 2102108.
[29] H. S. Lim, J. T. Han, D. Kwak, M. Jin, K. Cho, *J. Am. Chem. Soc.* **2006**, *128*, 14458.
[30] L. Lin, M. Wang, X. Wei, X. Peng, C. Xie, Y. Zheng, *Nano Lett.* **2016**, *16*, 7655.
[31] P. Wu, C. Wei, W. Yang, L. Lin, W. Pei, J. Wang, L. Jiang, *ACS Appl. Mater. Interfaces.* **2021**, *13*, 41220.
[32] L. Zhang, Y. Fan, J. Xie, X. Lai, T. Mao, J. Zhang, G. Zhang, L. Wang, *Chem. Eng. J.* **2023**, *474*, 145699.
[33] F. Miller, R. Chen, J. Fröch, Z. Fang, V. Tara, S. Geiger, A. Majumdar, *Nano Lett.* **2024**, *24*, 6844.

[34] F. Miller, R. Chen, J. E. Fröch, H. Rarick, S. Geiger, A. Majumdar, *Opt. Lett.* **2023**, *48*, 2385.
[35] C. Wu, H. Deng, Y.-S. Huang, H. Yu, I. Takeuchi, C. A. Ríos Ocampo, M. Li, *Sci. Adv.* **2024**, *10*, 1361.
[36] B. Wu, B. Zhang, W. Liu, Q. Lu, L. Wang, F. Chen, *Opt. Laser Technol.* **2022**, *145*, 107500.
[37] H. Liu, W. Dong, H. Wang, L. Lu, Q. Ruan, Y. S. Tan, R. E. Simpson, J. K. W. Yang, *Sci. Adv.* **2020**, *6*, eabb7171.
[38] K.-T. Lin, Y.-J. Chen, M.-R. Huang, V. K. Karapala, J.-H. Ho, J.-T. Chen, *Nano Lett.* **2020**, *20*, 5853.
[39] K. Ni, Q. Peng, E. Gao, K. Wang, Q. Shao, H. Huang, L. Xue, Z. Wang, *ACS Nano.* **2021**, *15*, 4747.
[40] G. B. González, T. O. Mason, J. P. Quintana, O. Warschkow, D. E. Ellis, J.-H. Hwang, J. P. Hodges, J. D. Jorgensen, *J. Appl. Phys.* **2004**, *96*, 3912.
[41] M. Inoue, T. Matsuoka, Y. Fujita, A. Abe, *Jpn. J. Appl. Phys.* **1989**, *28*, 274.
[42] M. Baum, H. Kim, I. Alexeev, A. Piqué, M. Schmidt, *Appl. Phys. A.* **2013**, *111*, 799.
[43] S. Elmas, Ş. Korkmaz, S. Pat, *Appl. Surf. Sci.* **2013**, *276*, 641.
[44] F. H. Alsultany, N. M. Ahmed, M. Z. Matjafri, *SNL* **2014**, *04*, 83.
[45] S. Lu, Y. Sun, K. Ren, K. Liu, Z. Wang, S. Qu, *Polymers.* **2017**, *10*, 5.
[46] M. Wang, A. Barnabé, Y. Thimont, J. Wang, Y. He, Q. Liu, X. Zhong, G. Dong, J. Yang, X. Diao, *Electrochim. Acta.* **2019**, *301*, 200.
[47] A. Solodar, A. Cerkauskaite, R. Drevinskas, P. G. Kazansky, I. Abdulhalim, *Appl. Phys. Lett.* **2018**, *113*, 081603.
[48] H. Lu, G. Han, J. Cao, M. Jin, Q. Ma, E. M. Akinoglu, X. Wang, L. Nian, G. Zhou, L. Shui, *Nanoscale Res. Lett.* **2020**, *15*, 8.
[49] R. A. Masitas, S. L. Allen, F. P. Zamborini, *J. Am. Chem. Soc.* **2016**, *138*, 15295.
[50] C. May, J. Strümpfel, *Thin Solid Films.* **1999**, *351*, 48.
[51] B. Han, K. Pei, Y. Huang, X. Zhang, Q. Rong, Q. Lin, Y. Guo, T. Sun, C. Guo, D. Carnahan, M. Giersig, Y. Wang, J. Gao, Z. Ren, K. Kempa, *Adv. Mater.* **2014**, *26*, 873.
[52] H. Cho, C. Wolf, J. S. Kim, H. J. Yun, J. S. Bae, H. Kim, J. Heo, S. Ahn, T. Lee, *Adv. Mater.* **2017**, *29*, 1700579.
[53] R. Pawlak, M. Lebioda, J. Rymaszewski, W. Szymanski, L. Kolodziejczyk, P. Kula, *Sensors.* **2016**, *17*, 51.
[54] M. Lebioda, R. Pawlak, *Physica Status Solidi.* **2016**, *213*, 1150.
[55] H. K. Lin, W. C. Hsu, *Appl. Surf. Sci.* **2014**, *308*, 58.
[56] J.-Y. Cheng, M.-H. Yen, W.-C. Hsu, J.-H. Jhang, T.-H. Young, *J. Micromech. Microeng.* **2007**, *17*, 2316.
[57] Y.-T. Cheng, J.-J. Ho, C.-K. Wang, W. Lee, C.-C. Lu, B.-S. Yau, J.-L. Nain, S.-H. Chang, C.-C. Chang, K. L. Wang, *Appl. Surf. Sci.* **2010**, *256*, 7606.
[58] F. Wang, Y. Yan, Q. Mu, P. Zhou, *Appl. Phys. A.* **2024**, *130*, 186.
[59] F. Kotz, A. S. Quick, P. Risch, T. Martin, T. Hoose, M. Thiel, D. Helmer, B. E. Rapp, *Adv. Mater.* **2021**, *33*, 2006341.
[60] L. Florea, E. Blasco, V. Mattoli, *Adv Funct Materials.* **2023**, *33*, 2305697.
[61] M.-F. Chen, *Optics and Lasers in Engineering.* **2012**, *50*, 491.
[62] O. Yavas, M. Takai, *J.Appl. Phys.* **1999**, *38*, 7131.
[63] M.-F. Chen, Y.-P. Chen, W.-T. Hsiao, Z.-P. Gu, *Thin Solid Films.* **2007**, *515*, 8515.
[64] H. W. Choi, D. F. Farson, J. Bovatsek, A. Arai, D. Ashkenasi, *Appl. Opt.* **2007**, *46*, 5792.
[65] C.-W. Cheng, J.-S. Chen, H.-H. Chen, *Mater. Manuf. Processes.* **2010**, *25*, 684.
[66] C.-W. Cheng, C.-Y. ing Lin, W.-C. Shen, Y.-J. Lee, J.-S. Chen, *Thin Solid Films.* **2010**, *518*, 7138.
[67] C.-W. Cheng, C.-Y. Lin, *Appl. Surf. Sci.* **2014**, *314*, 215.
[68] J. Hu, Z.-Z. Li, Y.-Y. Zhao, Y.-S. Xu, L. Wang, M. Han, L. Hyde, S. H. Ng, L. Wang, S. Juodkazis, *Nanomaterials.* **2022**, *12*, 4092.
[69] G. Folcher, H. Cachet, M. Froment, J. Bruneaux, *Thin Solid Films.* **1997**, *301*, 242.
[70] A. Kraft, H. Hennig, A. Herbst, K.-H. Heckner, *J. Electroanal. Chem.* **1994**, *365*, 191.
[71] J. Stotter, Y. Show, S. Wang, G. Swain, *Chem. Mater.* **2005**, *17*, 4880.
[72] C. C. P. Cid, E. R. Spada, M. L. Sartorelli, *Appl. Surf. Sci.* **2013**, *273*, 603.
[73] H. Wang, C. Zhong, C. Jiang, X. Gu, J. Li, Y. Jiang, *Acta. Phys. Chim. Sin.* **2009**, *25*, 835.
[74] W. Hao, Z. Cheng, L.i Jin, J. Yiming, presented at *2008 International Conf. on Electronic Packaging Technology & High Density Packaging*, IEEE, Shanghai **2008**, 1–4.
[75] W. Gao, S. Cao, Y. Yang, H. Wang, J. Li, Y. Jiang, *Thin Solid Films.* **2012**, *520*, 6916.
[76] M. Senthilkumar, J. Mathiyarasu, J. Joseph, K. L. N. Phani, V. Yegnaraman, *Mater. Chem. Phys.* **2008**, *108*, 403.
[77] M. A. Martínez, J. Herrero, M. T. Gutiérrez, *Electrochim. Acta.* **1992**, *37*, 2565.
[78] E. Matveeva, *J. Electrochem. Soc.* **2005**, *152*, H138.
[79] L. Liu, S. Yellinek, I. Valdinger, A. Donval, D. Mandler, *Electrochim. Acta.* **2015**, *176*, 1374.
[80] L. Rodríguez-Suné, M. Scalora, A. S. Johnson, C. Cojocaru, N. Akozbek, Z. J. Coppens, D. Perez-Salinas, S. Wall, J. Trull, *APL Photonics.* **2020**, *5*, 010801.
[81] A. Anopchenko, L. Tao, C. Arndt, H. W. H. Lee, *ACS Photonics.* **2018**, *5*, 2631.
[82] M.d. A. Badsha, Y. C. Jun, C. K. Hwangbo, *Opt. Commun.* **2014**, *332*, 206.
[83] F. Dell'Ova, K. Malchow, N. Pocholle, R. Chassagon, O. Heintz, G. Colas Des Francs, E. Dujardin, A. Bouhelier, *EPJ Web Conf.* **2023**, *287*, 06013.
[84] W. Jia, M. Liu, Y. Lu, X. Feng, Q. Wang, X. Zhang, Y. Ni, F. Hu, M. Gong, X. Xu, Y. Huang, W. Zhang, Y. Yang, J. Han, *Light Sci. Appl.* **2021**, *10*, 11.
[85] X. Feng, X. Chen, Y. Lu, Q. Wang, L. Niu, Q. Xu, X. Zhang, J. Han, W. Zhang, *Adv. Opt. Mater.* **2023**, *11*, 2201628.
[86] X. Feng, X. Zhang, H. Qiu, Q. Xu, W. Zhang, J. Han, *Appl. Phys. Lett.* **2024**, *124*, 171101.
[87] D. H. Van Dorp, S. Arnauts, M. Laitinen, T. Sajavaara, J. Meersschaut, T. Conard, J. J. Kelly, *Appl. Surf. Sci.* **2019**, *465*, 596.
[88] C. J. Lee, H. K. Lin, C. H. Li, L. X. Chen, C. C. Lee, C. W. Wu, J. C. Huang, *Thin Solid Films.* **2012**, *522*, 330.

Supporting Information

Rewritable ITO Patterning for Nanophotonics

Xinqin Liu, Pan Peng, Zhenyang Zhang, Xiangyu Zhao, Wenyu Chen, Shiyuan Liu, and Jinlong Zhu**

State Key Laboratory of Intelligent Manufacturing Equipment and Technology, Huazhong University of Science and Technology, Wuhan 430074, People's Republic of China
Research Institute of Huazhong University of Science and Technology Shenzhen, Shenzhen 518057, China
Optics Valley Laboratory, Wuhan, Hubei 430074, People's Republic of China
E-mail: jinlongzhu03@hust.edu.cn

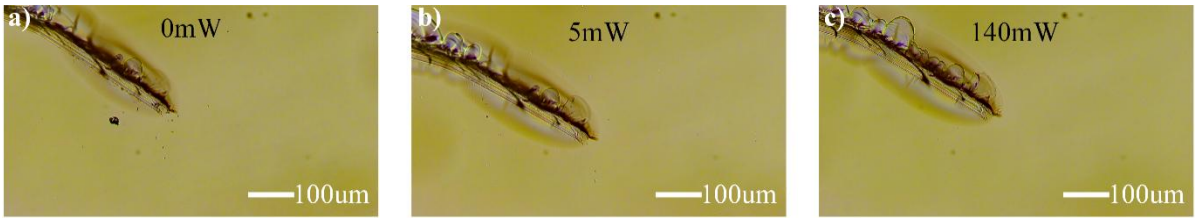

Figure S1. Direct CW laser writing on an ITO thin film without electrochemical assistance. As can be observed, it cannot generate any patterns at laser powers of a) 0 mW, b) 5 mW, and even c) 140 mW. Diamond pen scratches were used solely to locate the position. These results indicate that ITO thin film cannot be directly patterned by CW laser with power below 140 mW.

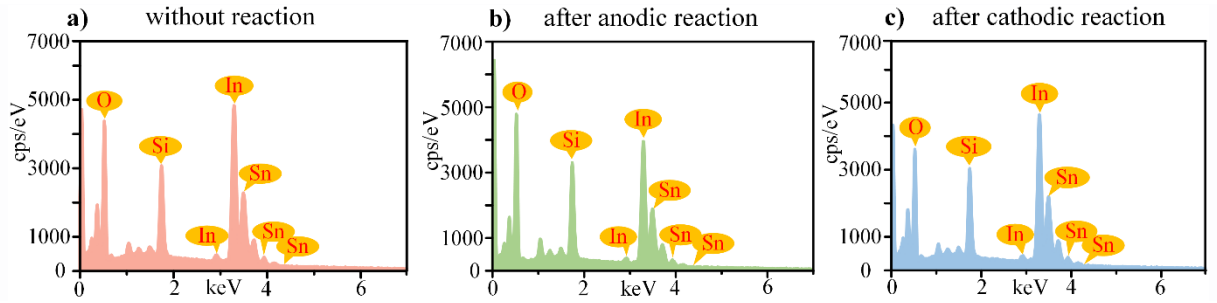

Figure S2. EDS analysis of ITO thin film before and after electrochemical reactions. a) EDS analysis of the unreacted ITO thin film, which serves as a reference. b) EDS analysis of the ITO thin film after anodic reaction. c) EDS analysis of the ITO thin film after cathodic reaction.

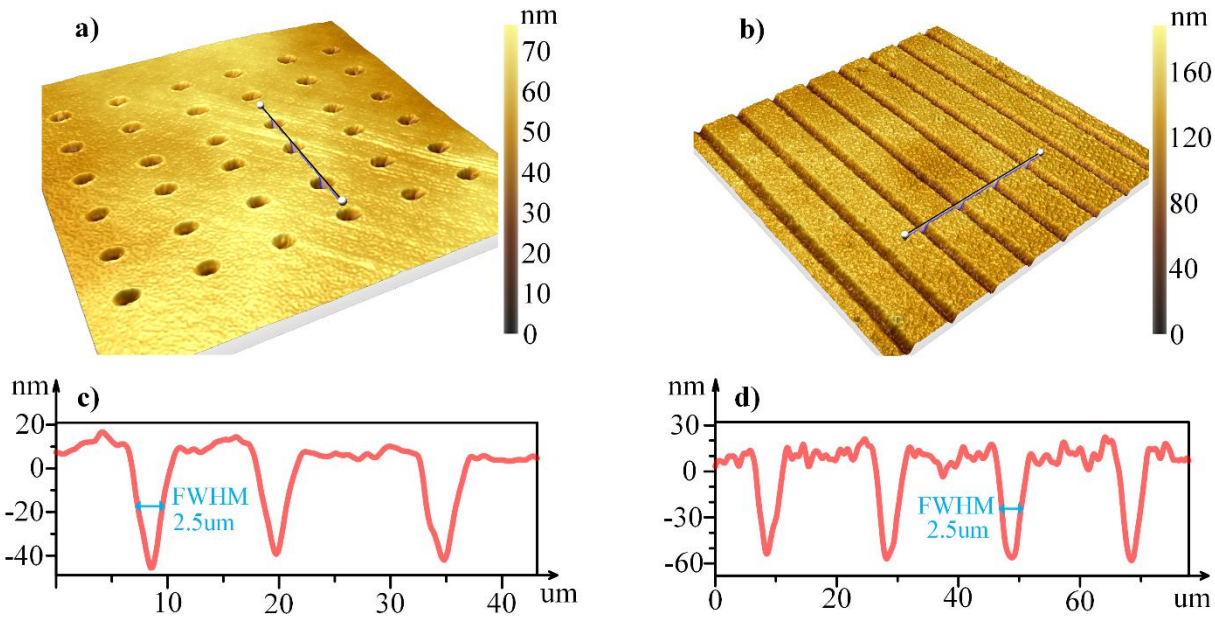

Figure S3. 3D images and the corresponding cross-sections of the ITO nanopatterns under anodic a, c) and cathodic b, d) reactions.

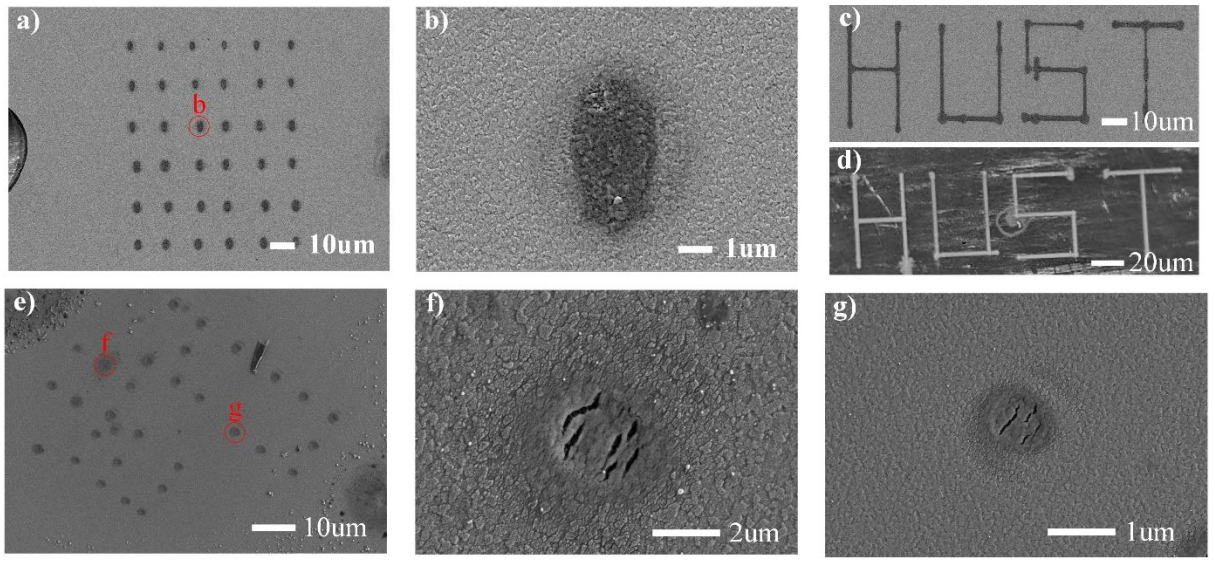

Figure S4. ITO surface patterning results under anodic polarization and cathodic polarization, respectively. a) SEM image of a 6×6 dot array. b) Detailed SEM view of a single dot from a). c) SEM image of a “HUST” logo. d) Optical image of the “HUST” logo. e) SEM image of a dot pattern with cracks. f,g) Detailed SEM views of cracked dots from e).

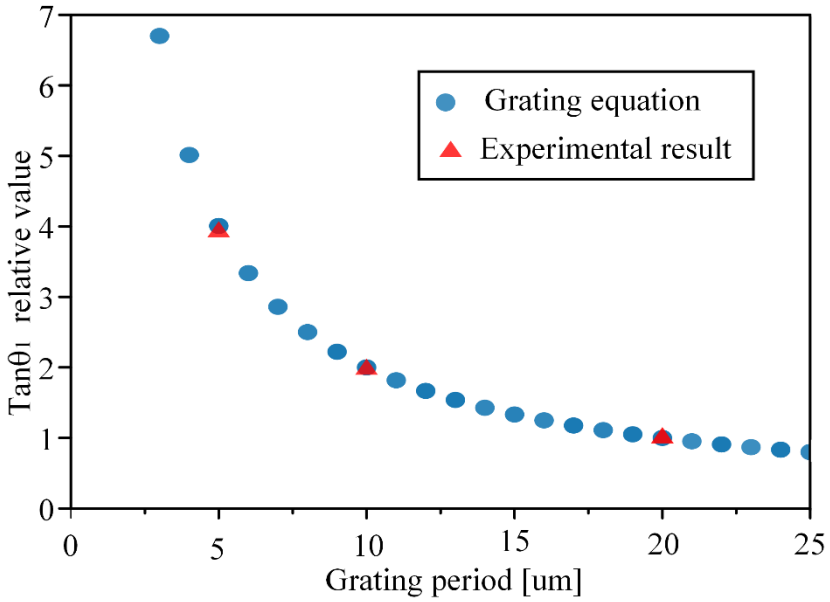

Figure S5. The theoretical (blue circle) and experimental (red triangle) diffraction angles, which were calculated according to the grating equation and experimental measurements, respectively.

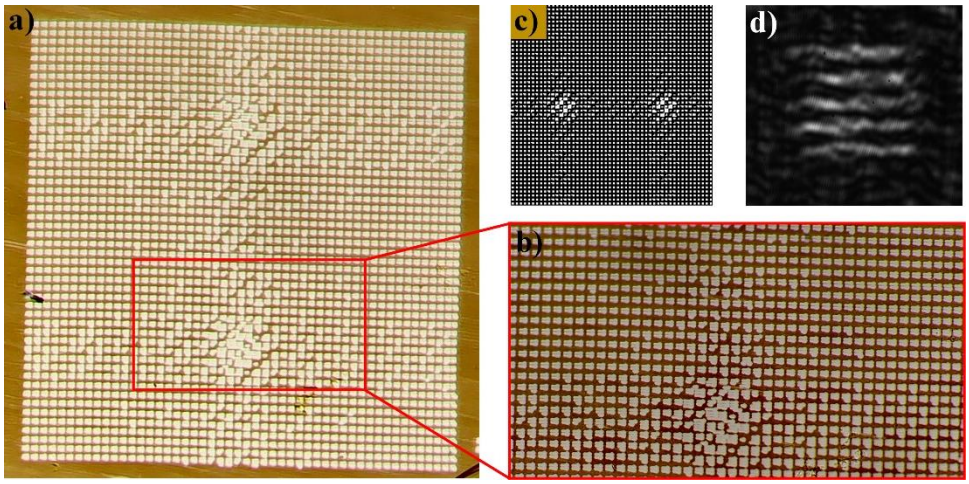

Figure S6. a) The fabricated holography mask and b) the zoomed-in view showing the feature details. c) The computer-generated hologram with 200×200 pixels. d) The holographic reconstruction image (i.e., raster lines) captured by the camera in Figure 3d.

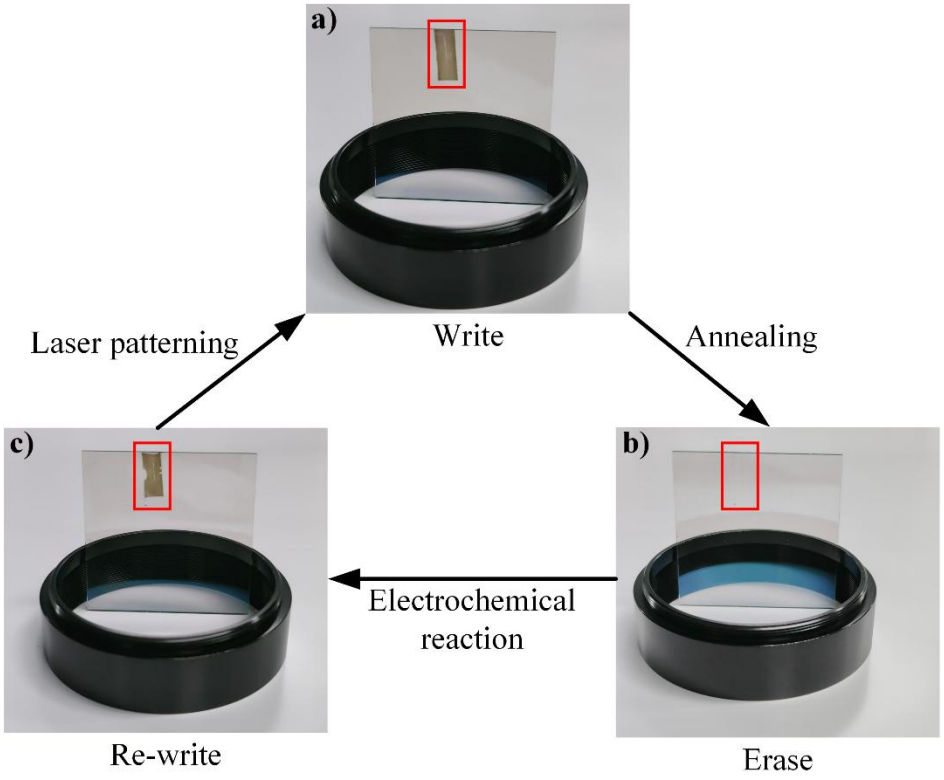

Figure S7. Schematic of the reversible ITO patterning under cathodic polarization. a) Electrochemical reaction generates a bronze indium layer on the ITO thin film followed by CW laser writing. b) Annealing erases the patterns and restores the transparency of ITO thin film. c) Direct CW laser writing assisted by electrochemical reaction rewrites patterns on ITO thin film, turning the surface bronze again.